

Ion-atom differential cross sections at intermediate energies

R. E. Olson

Physics Department, University of Missouri—Rolla, Rolla, Missouri 65401

(Received 25 October 1982)

The classical-trajectory Monte Carlo method has been used to calculate $H^+ + H(1s)$ electron-capture and ionization differential cross sections in the range 25–200 keV. The results indicate the importance of including excited product states to describe the small-angle electron-capture scattering. Angular scattering of the electron removed by the ionization process has been studied as a function of ejected-electron velocity v_e . The classical calculations are in reasonable agreement with coupled-channel results of Shakeshaft [Phys. Rev. A **18**, 1930 (1978)] as to the “electron capture to the continuum” (ECC) component of the ionization process where this term is defined as the ejected electron being more closely centered to the projectile than the target nucleus after the collision. The ECC cross section σ_{ECC} was studied as a function of collision energy (50–500 keV/amu) and projectile charge state ($q = 1-10$). At high energies, σ_{ECC} scales as $q^{2.3}/E^{2.5}$. The maximum value for σ_{ECC} was determined to be an energy $E_{\text{max}} \cong (56 \text{ keV/amu})q^{0.4}$. Restricting the ECC component to small electron-scattering angles, $\theta_{\text{lab}} \leq 5^\circ$, and electron-ejection velocities $v_e = v_p(1.0 \pm 0.1)$, where v_p is the projectile velocity, indicates this process is a minor component of the total ionization cross section at intermediate energies.

I. INTRODUCTION

Recently, there has been considerable interest in the angular scattering induced by ion-atom collisions at intermediate energies. The study of such processes directly probes the impact-parameter dependence of the transition under study and provides a sensitive test for theoretical methods. Experimental observations made by the groups of Rudd,¹ Sellin,² Park,³ and others have prompted a considerable amount of theoretical interest. Calculations and formulations performed by such workers as Macek,⁴ Salin,⁵ and Shakeshaft^{6,7} have provided much of the insight into the physical collision mechanisms.

It is the purpose of this paper to extend the work of others and provide “exact” classical calculations of some of the collision processes. These calculations are made at intermediate energies ($25 \text{ keV/amu} \leq E \leq 500 \text{ keV/amu}$) where perturbation methods such as the various Born approximations are invalid. On the other hand, coupled-channel calculations require exhaustive numerical techniques with a large number of coupled channels to obtain accurate cross sections at intermediate energies.⁶ Classical calculations, while much simpler to implement, must employ several approximations with regard to the energy levels and radial distributions of the bound electron.

The classical-trajectory Monte Carlo (CTMC) method provides an exact classical description of the

three-body, three-dimensional scattering for electron-capture and ionization reactions:

$$A^{q+} + B \rightarrow \begin{cases} A^{(q-1)+} + B, & (1a) \\ A^{q+} + B^+ + e, & (1b) \end{cases}$$

where the ion A^{q+} is fully stripped and B is atomic hydrogen. The CTMC method has been very valuable in predicting the *total* cross sections^{8,9} for (1) and should provide insight into the angular scattering mechanisms. It should be noted that CTMC calculations by Banks *et al.*,¹⁰ preceded the extensive coupled-channel calculations of Shakeshaft⁶ in the prediction of a large “electron capture to the continuum” (ECC) component in the ionization cross section for $H^+ + H$ which is found to maximize at $E \cong 50 \text{ keV}$. Similar to Refs. 6 and 10, we will define the ECC component of the ionization cross section as the ejected electron in reaction (1b) being found to be more closely centered to the projectile than the target nucleus after the collision.

In order to benchmark the CTMC calculations, we will first compare the theoretical results to measured $H^+ + H$ differential cross sections for angular scattering in electron-capture collisions¹¹ and energy-loss measurements for the ionization process.¹² The angular scattering of the heavy particles after ionization are given for future comparison to experimental data. Extension is then made to ECC studies for reaction (1b) when A^{q+} is fully stripped ($1 \leq q \leq 10$), B is atomic hydrogen, and the energy

range is 50–500 keV/amu. The energy and charge-state dependence of the ECC total cross sections are presented. Doubly differential ECC cross sections (in angle and ejection velocity of the electron) are also given for the $H^+ + H$ system.

II. THEORETICAL METHOD

The CTMC method has been fully described by Percival and Richards,¹³ Olson and Salop,¹⁴ and others. The method consists of solving Hamilton's equations of motion for a three-body three-dimensional system. The classical Hamiltonian is given by

$$H = \sum_{i=1}^3 p_i^2/2m_a + \sum_{i=4}^6 p_i^2/2m_b + \sum_{i=7}^9 p_i^2/2m_c + V(q_1, q_2, \dots, q_9), \quad (2)$$

where m_a , m_b , and m_c are the masses of the three particles, p_i and q_i their respective momenta and coordinates, and V the Coulomb potentials between the point charges. Eighteen first-order coupled differential equations arise to follow the time dependence of the three particles' motions

$$\frac{dq_i}{dt} = \frac{\partial H}{\partial p_i} \quad (3)$$

and

$$\frac{dp_i}{dt} = -\frac{\partial H}{\partial q_i}. \quad (4)$$

Six random numbers are used to initialize each trajectory and determine the impact parameter, and the plane and eccentricity of the electron's orbit about the target nucleus. Several thousand trajectories are computed, and the cross sections for a specific event are calculated by

$$\sigma_R = \pi b_{\max}^2 \left[\frac{N_R}{N} \right], \quad (5)$$

with a one-standard deviation error limit given by

$$\Delta\sigma_R = \sigma_R \left[\frac{(N - N_R)}{NN_R} \right]^{1/2}. \quad (6)$$

In Eqs. (5) and (6), N is the total number of trajectories calculated for impact parameters less than b_{\max} , and N_R is the number of trajectories that satisfy the criteria for a given collision process such as capture, ionization, etc.

From Eq. (6), it is apparent that the CTMC method is not applicable to a minor collision process since the error limits become unacceptable to obtain meaningful results. To a good approximation, the

statistical error limit can be written $\Delta\sigma \approx \sigma/N_R^{1/2}$. For 10% error bars $N_R \approx 100$, so that a process occurring in only 1% of the collisions requires the computation of 10 000 trajectories. In the calculations presented here, we found it necessary to compute 10 000–60 000 trajectories at each energy in order to obtain good statistics for the differential cross sections.

The CTMC method does not account for interference or tunneling effects. However, the method is nonperturbative and explicitly considers all three-body three-dimensional effects. Of importance for our application is that the Rutherford scattering of two charged particles is the same in both classical and quantum-mechanical frameworks.

Since the momenta and coordinates of each particle are known throughout the collision, differential cross sections can be readily calculated. In this paper, we have used the Cartesian coordinates of the particles after the collisions to determine the scattering angles. Convergence was verified by integrating in stages to $100a_0$ past the collision zone. The momenta components of the particles can also be used to determine the scattering angles. However, one must use caution when investigating the electron-capture process, since the orbital momentum of the captured electron will be contained in the calculated momenta and must be removed before the angle determination. Failure to do this subtraction will lead to differential cross sections which are not sufficiently forwardly peaked and are artificially broadened to large angles.

Estimates of the excited-state product distributions after electron capture, reaction (1a), can be determined from the energy of the captured electron relative to the projectile E_{ep} to obtain a classical principal quantum number

$$n_c = q/(-2E_{ep})^{1/2}. \quad (7)$$

The classical values are "quantized" to a specific n level if they lie between the limits

$$\begin{aligned} [(n-1)(n-\frac{1}{2})n]^{1/3} \leq n_c \\ \leq [n(n+\frac{1}{2})(n+1)]^{1/3}. \end{aligned} \quad (8)$$

Mackeller and Becker¹⁵ derived relationship (8) and have shown the phase space per bin equals the n^2 multiplicity of a given quantal n level. Equation (8) has also been tested¹⁶ on a large series of reactions of type (1a).

III. CALCULATIONAL RESULTS

A. Electron capture

Electron-capture differential cross sections are presented in Fig. 1. These cross sections include all

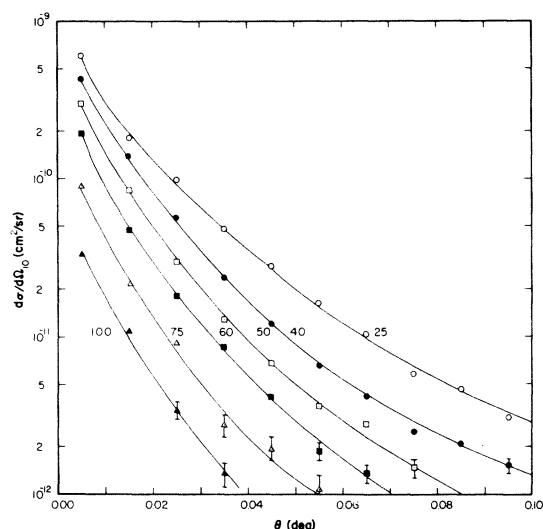
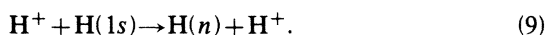


FIG. 1. Calculated electron-capture differential cross sections for projectile energies from 25 to 100 keV. Calculations include capture to all excited levels for the $H^+ + H(1s) \rightarrow H(n) + H^+$ reaction. Both the differential cross section and scattering angle are in the center-of-mass frame. Error bars are given when one-standard deviation exceeds 10%. Total cross sections corresponding to these differential cross sections are presented in Table I.

possible excited-state products in the reaction



The overall magnitude of the differential cross sections mirror the total cross sections (Table I), with the shapes becoming slightly more sharply peaked as the collision energy is increased.

The 25- and 60-keV results have been compared to experimental data by Park.³ At 25 keV, our calculated values lie below the data at small angles. This behavior is also reflected in the total electron-capture cross section, which is $\sim 25\%$ lower than

TABLE I. Total cross sections for $H^+ + H$ collisions which correspond to the calculated differential cross sections presented in this paper.

E (keV)	σ_{10} (10^{-16} cm ²)	σ_{ion} (10^{-16} cm ²)
25	3.02	
40	1.76	
50	1.06	1.40
60	0.64	1.53
75	0.30	1.44
100	0.12	1.20
125		0.97
150		0.84
175		0.76
200		0.66

the accepted experimental value.¹⁷ Such behavior is indicative of the deficiency in the classical description of the radial distribution of the target's hydrogenic electron. Although the classical momentum distribution reproduces the quantum-mechanical result, the radial distribution does not allow the electron to penetrate into the classically forbidden regime ($r > 2a_0$). Thus, small-angle large-impact-parameter collisions are not well described by the CTMC method. As the collision energy increases above 25 keV, the range of impact parameters contributing to the electron-capture process decreases, so that one can expect more accurate results.

Eichenauer *et al.*¹⁸ have tried to remedy the CTMC method with the use of a Wigner distribution to describe the electron's orbit. These authors' results lie below ours and the experimental data at small angles by about a factor of 4. We are able to reproduce their values by determining the scattering angles from the momenta of the projectile after the collision and ignoring the contribution to the angles from the orbital angular momentum components.

In Fig. 2 we display in detail the 60-keV calculations. The differential cross section for capture to all states is in reasonable accord with the measurements of Martin *et al.*¹¹ Also shown are CTMC calculations for capture to the $1s$, $n=2$ and 3 levels.

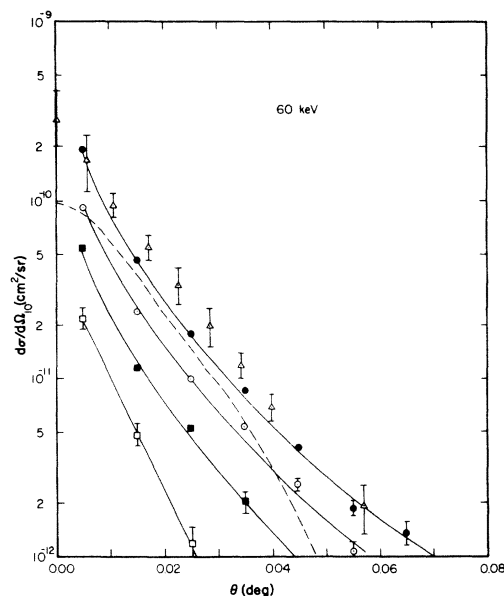


FIG. 2. Electron-capture differential cross sections for the $H^+ + H(1s)$ reaction in center-of-mass coordinates and a projectile energy of 60 keV. CTMC calculations for capture to all states are given by the solid circles; for capture to $H 1s$ \circ ; for capture to $H(n=2)$, \blacksquare ; and for capture to $H(n=3)$, \square . Experimental values of Martin *et al.* (Ref. 11) are denoted by Δ and the calculations of Shake-shaft (Ref. 19) for capture to $H 1s$ are denoted by $---$.

Equations (7) and (8) were used in the determination of these cross sections. The calculations indicate the importance of including excited product states in the computation of the electron-capture cross sections, especially at the small angles which are determined by "soft," large-impact-parameter collisions. Similar behavior is noted in the $n \geq 2$ contribution to the total cross section¹⁶ at 60 keV, which is approximately 40%.

The calculations of Shakeshaft¹⁹ for capture to the H1s are also displayed in Fig. 2. The calculations of Shakeshaft are based on a straight-line, coupled-channel calculation⁶ of the transition amplitudes and the use of the eikonal method to determine the differential cross sections. The agreement of the CTMC and quantum-mechanical H1s cross sections is within $\pm 50\%$, except at angles around 0.06° at which Shakeshaft¹⁹ notes there is a dip in the differential cross section. The CTMC results do not indicate this dip, nor do the measurements¹¹ which are for capture to all electronic levels but are dominated by the H1s contribution at the larger angles.

An interesting behavior observed in the CTMC calculations is contributions from both positive and negative angle deflections. At the smallest angles, $\theta_{cm} < 0.04^\circ$, we note that almost one-half of the cross section arises from negative angle deflections. Such behavior can be interpreted as follows: in large-impact-parameter collisions the projectile is slightly attracted to the electron before the capture event by the Coulomb force between the positively charged projectile and the electron. The target nucleus,

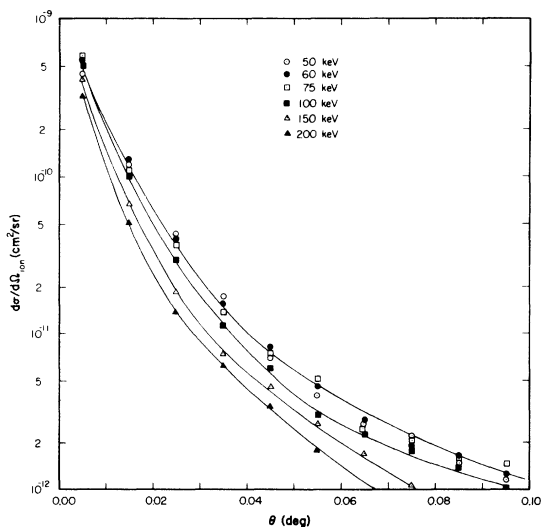
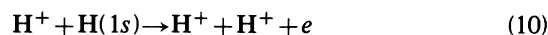


FIG. 3. Ionization differential cross sections for the $H^+ + H$ reaction in center-of-mass coordinates and projectile energies in the range of 50–200 keV.

while being much more massive, is far removed from the electron-capture center and, thus, can be considered a spectator to the collision event. This mixture of both positive and negative angle deflections to the same scattering angle makes it very difficult to uniquely relate a specific scattering angle to a given impact-parameter collision.

B. Ionization

Differential cross sections for the ionization reaction



are given in Fig. 3 where the scattering of the heavy particles is followed. Within statistical errors generated by the CTMC method, the 50-, 60-, and 75-keV results are almost identical. As the collision energy further increases, the magnitude of the cross sections decreases and the cross sections become more forwardly peaked. The general behavior of the differential cross sections is mirrored by the total cross sections given in Table I. No structure is observed on the cross sections and experimental data are lacking for a direct test of the calculations.

There are data available, however, for energy-loss

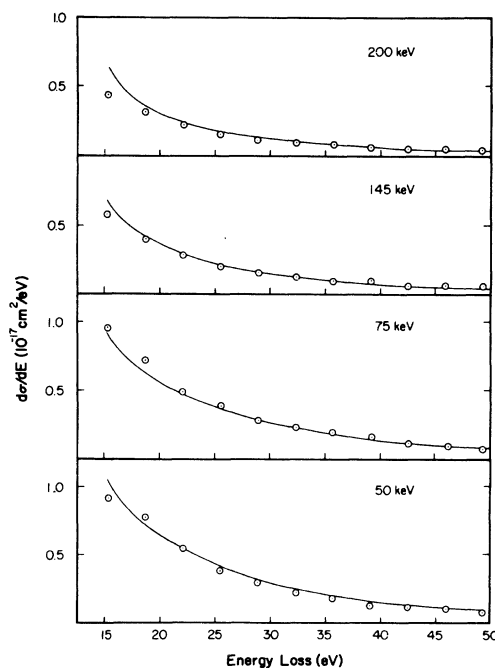


FIG. 4. Calculated energy-loss spectra for ionization in the $H^+ + H$ reaction, \circ . Calculations are compared to the experimental data of Park *et al.* (Ref. 12), denoted by the lines, which have been normalized to the total cross sections by Shah and Gilbody (Ref. 20). Projectile energies are given in the figure.

spectra in the $H^+ + H$ ionization reaction. The measurements were performed by Park *et al.*¹² at 25-, 50-, 75-, 145-, and 200-keV projectile energies. Since the total cross sections deduced from the energy-loss spectra are larger than currently accepted values, we have normalized the data of Park *et al.* to the most recent measurements of Shah and Gilbody.²⁰ The normalization factors we obtained from the ratio of total cross sections and used to multiply the experimental energy-loss spectra were 0.56, 0.57, 0.73, and 0.70 for projectile energies of 50-, 75-, 145-, and 200-keV, respectively. The CTMC ionization total cross sections given in Table I are all within 10% of the Shah and Gilbody measurements.

The comparison of experimental and calculated energy-loss spectra is given in Fig. 4. The agreement is good except near threshold, 13.6 eV, for the 200-keV case. We should note that within the statistical uncertainties of the CTMC calculations, no sharp peak attributable to ECC was observed in which the electron is ejected at the same velocity as the projectile. The peak would be expected to occur at an energy loss corresponding to an electron ejection velocity equal to that of the projectile, which is 27.2 and 40.8 eV for the 50-, and 75-keV results, respectively. However, no attempt was made to emphasize the ECC peak by restricting the energy-loss spectra calculations to only those events where the

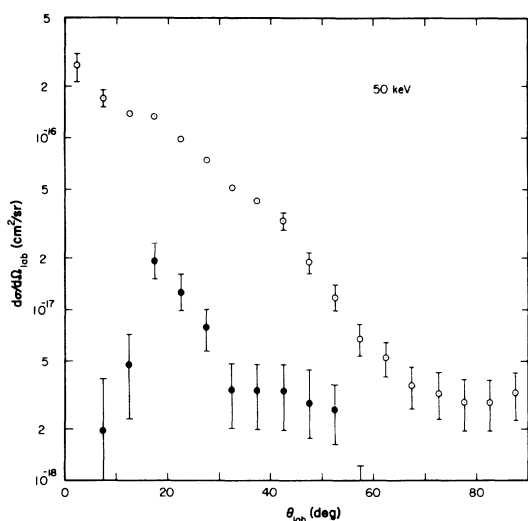


FIG. 5. Differential cross sections for the scattering of the ejected electron in the $H^+ + H$ ionization reaction. Projectile energy is 50 keV and the values are presented in laboratory coordinates. Open circles denote the cross section for electrons ejected to all possible energies, while the solid circles give the cross section for only those electrons that are ejected with a velocity within $\pm 10\%$ of that of the projectile.

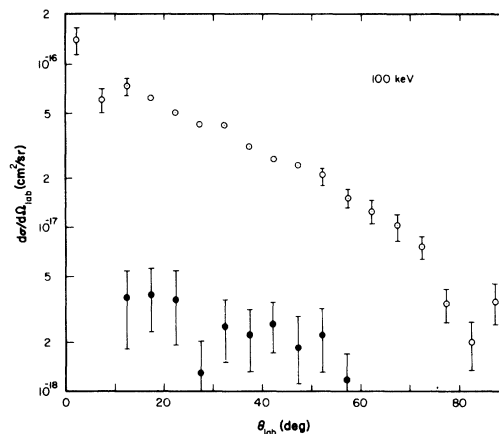


FIG. 6. Same as Fig. 5 except 100 keV.

electrons are scattered to small angles. In Sec. III C the differential cross sections for the ejected electron are presented.

C. Electron capture to the continuum

In order to follow the ECC component of the ionization process [(10)] more easily, it is instructive to plot the differential cross sections for the electron ejected by the collision. In Figs. 5–7, we show CTMC calculations for projectile energies of 50, 100, and 200 keV. Error bars are given when a 1-s.d. uncertainty exceeds 10%.

The open circles depict electron-ejection differential cross sections summed over all possible ejection energies. The integral of these cross sections yields the total cross sections given in Table I. The differential cross sections in the laboratory system are forwardly peaked with a tendency to become isotropic as the projectile energy increases.

Of interest, however, is the ECC component which we have restricted to include only electron-ejection velocities v_e that are within $\pm 10\%$ of the

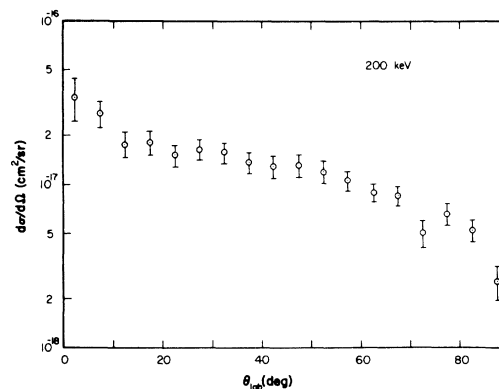


FIG. 7. Same as Fig. 5 except 200 keV.

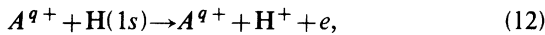
projectile's velocity v_p

$$v_e = v_p(1.0 \pm 0.1). \quad (11)$$

Calculated cross sections for this ECC component are shown in Figs. 5 and 6 for 50- and 100-keV collisions. At 200 keV, there were so few counts that the results are meaningless. It is important to note that we could not find any counts for scattering at angles less than 5° . Thus, the forwardly scattered ECC component appears to be very small at intermediate collision energies. Such behavior translates to these latter electrons being eventually captured to Rydberg levels of the projectile ion. Irrespective of the scattering angles, the percentage of the ionization cross section that satisfies Eq. (11) is calculated to be 8.6%, 5.6%, and 3.0% at 50, 100, and 200 keV, respectively.

We did note, however, a considerable number of small-angle scattering events for ejected-electron velocities approximately equal to one-half the projectile velocity. These electrons are ones that are left stranded equidistant between the projectile- and target-nucleus ions and are balanced in place by the attractive Coulomb forces of both ions.

An attribute of the CTMC method is that it can be easily applied to a large variety of collision systems. Of interest is the scaling relationships versus projectile energy and charge state of the ECC total cross sections.^{2,21} In this study, we have defined the ECC total cross section to include simply that component of the total ionization cross section where the ejected electron is found centered closer to the projectile than the target nucleus after the collision. We have investigated the class of reactions



where A^{q+} is a fully stripped ion in charge state $1 \leq q \leq 10$ and the projectile energy ranges from 50 to 500 keV/amu.

After calculating the ECC total cross sections, σ_{ECC} , it became readily apparent that at the higher energies the cross sections were scaling as $q^{2.3}/E^{2.5}$. Moreover, the maximum value of σ_{ECC} was proportional to $q^{1.3}$. Thus, a reduced plot of $\sigma_{\text{ECC}}/q^{1.3}$ vs $E^{2.5}/q$ is appropriate and should display a slope of -1 on a log-log scale at high energies and plateau to a constant value at intermediate energies.

Such a reduced plot is shown in Fig. 8. All the high-energy values coalesce to a common line for $[E(\text{keV}/\text{amu})]^{2.5}/q \geq 10^5$. The resulting analytical form for the ECC total cross section is

$$\sigma_{\text{ECC}}(\text{cm}^2) = \frac{4 \times 10^{-12} q^{2.3}}{[E(\text{keV}/\text{amu})]^{2.5}}, \quad (13)$$

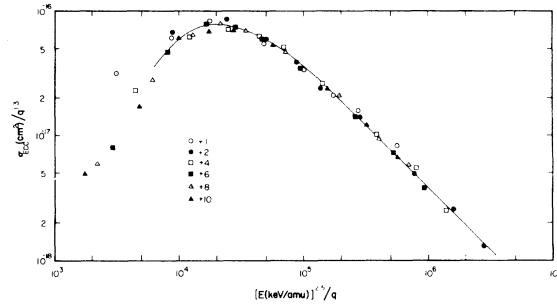


FIG. 8. Electron capture to the continuum total cross sections reduced to a common curve by plotting $\sigma_{\text{ECC}}/q^{1.3}$ vs $E^{2.5}/q$. CTMC calculations are valid for projectile energies in the range 50–500 keV/amu and fully stripped ions in charge states $1 \leq q \leq 10$ colliding with atomic hydrogen.

where q is the charge state of the incident ion. A maximum in the ECC total cross section is found at

$$E_{\text{max}}(\text{keV}/\text{amu}) = 56q^{0.4}, \quad (14)$$

with the magnitude

$$\sigma_{\text{ECC}}^{\text{max}}(\text{cm}^2) = 8 \times 10^{-17} q^{1.3}. \quad (15)$$

It is stressed that the above parametrizations were obtained from calculations performed in the 50–500-keV/amu range and for incident ion charge states $q = 1-10$.

The physical interpretation of the results presented in Fig. 8 can be made if we consider the ECC cross section as a combination electron-capture–ionization process; i.e., continuation of the electron capture to a continuum state of the projectile. Our CTMC calculations indicated that the ECC cross section is roughly proportional to the product of the square roots of the electron capture $\sigma_{q,q-1}$ and ionization σ_{ion} cross sections:

$$\sigma_{\text{ECC}} \propto (\sigma_{q,q-1} \sigma_{\text{ion}})^{1/2}. \quad (16)$$

At high energies, CTMC calculations and experimental results^{22–25} indicate the electron-capture cross section scales roughly as

$$\sigma_{q,q-1} \propto q^3/E^{4.5}, \quad (17)$$

while the ionization cross sections⁹ are proportional to q^2/E

$$\sigma_{\text{ion}} \propto q^2/E. \quad (18)$$

In Eq. (18), note the CTMC results do not yield the quantum-mechanical $\ln E$ factor, yet comparison with experiment indicates the data are reasonably reproduced.⁹ Inserting Eqs. (17) and (18) into Eq. (16) yields $\sigma_{\text{ECC}} \propto q^{2.5}/E^{2.75}$, a result almost duplicated by our calculations [Eq. (13)].

The maximum in the ECC cross section occurs at

a projectile energy where the ionization and electron-capture cross sections are approximately equal, as seen from the results of Ref. 14. At higher energies, the electron-capture cross section decreases rapidly, while at lower energies the ionization cross section is decreasing, leading to a maximum in Eq. (16). The charge and energy dependence of σ_{ECC} at the maximum is not easily predicted. In the energy region of the maximum, the charge dependence of the electron-capture cross section^{22,23} is $\sim q^2$, while the ionization cross section varies approximately linearly²⁶ with charge state, thus, from Eq. (16) we would predict an $\sim q^{1.5}$ dependence in approximate accord with Eq. (15).

The CTMC calculations of the ECC total cross sections for atomic hydrogen targets are in partial agreement with experimental data on rare-gas targets. At high energies, 2.5 MeV/amu, Breinig *et al.*² find the ECC total cross section for fully stripped ions, $1 \leq q \leq 14$, colliding with Ar scales as $q^{2.3 \pm 0.3}/v^{4.3 \pm 0.3}$, consistent with Eq. (13). However, for He targets, the velocity scaling is found to be $v^{-8.4 \pm 0.6}$; at present we have no explanation for the latter difference except that the small-angle ECC differential cross sections may depend differently on velocity than our calculated total cross sections. The maximum in the ECC cross section has been investigated by Rødbro and Andersen.²⁷ These authors investigated collisions of protons in He, Ar, and H₂ and found $\sigma_{\text{ECC}}^{\text{max}}$ to occur at a velocity $v \approx 1.4v_0$, where v_0 is the orbital velocity of the electron which is ejected. For an atomic hydrogen target, the above velocity corresponds to a proton energy of 49 keV, very close to the 56-keV value found here [Eq. (14)].

The coupled-state calculations of Shakeshaft⁶ on the H⁺ + H system place the maximum of the ECC cross section at 40 keV with a magnitude of $9 \times 10^{-17} \text{ cm}^2$. We are in general agreement with

Shakeshaft's value except the CTMC results are shifted to slightly higher energies, $E_{\text{max}} \cong 56 \text{ keV}$ and $\sigma_{\text{ECC}}^{\text{max}} = 8 \times 10^{-17} \text{ cm}^2$. As expected we are in complete agreement with the H⁺ + H CTMC results of Banks *et al.*¹⁰

IV. CONCLUDING REMARKS

The CTMC method has been used to investigate the heavy particle and electron angular scattering in H⁺ + H electron capture and ionization collisions. The CTMC calculations are successfully compared to experimental data of electron-capture differential cross sections¹¹ and to energy-loss spectra¹² for the ionization process. The angular scattering of the electrons ejected after the ionization reactions also have been calculated and are forwardly peaked, becoming almost isotropically scattered at the highest energy of 200 keV. The component of the ejected electrons whose velocities are close to that of the projectile have been followed and the small electron scattering angle $\theta_{\text{lab}} \leq 5^\circ$ contribution to the total ionization cross section is negligible.

Electron capture to the continuum total cross sections are also calculated for fully stripped ions in charge states $1 \leq q \leq 10$ colliding with atomic hydrogen at 50–500 keV/amu. The CTMC results can be presented on a reduced plot of $\sigma_{\text{ECC}}/q^{1.3}$ vs $E^{2.5}/q$. The ECC cross sections maximize at a projectile energy of $56q^{0.4} \text{ (keV/amu)}$ with a magnitude of $8 \times 10^{-17} q^{1.3} \text{ (cm}^2\text{)}$. At high energies the cross sections decrease as $q^{2.3}/E^{2.5}$. The CTMC results are in partial agreement with the measurements of Breinig *et al.*² and Rødbro and Andersen.²⁷

ACKNOWLEDGMENTS

The author would like to thank the Physics Division of the U.S. Office of Naval Research for support of this research.

¹G. B. Crooks and M. E. Rudd, *Phys. Rev. Lett.* **25**, 1599 (1970).

²M. Breinig, S. B. Elston, S. Hultdt, L. Liljeby, C. R. Vane, S. D. Berry, G. A. Glass, M. Schauer, I. A. Sellin, G. D. Alton, S. Datz, S. Overbury, R. Laubert, and M. Sutter, *Phys. Rev. A* **25**, 3015 (1982).

³J. T. Park, *Electronic and Atomic Collisions*, edited by S. Datz (North-Holland, Amsterdam, 1982), pp. 109–121.

⁴J. Macek, *Phys. Rev. A* **1**, 235 (1970).

⁵A. Salin, *J. Phys. B* **2**, 631 (1969).

⁶R. Shakeshaft, *Phys. Rev. A* **18**, 1930 (1978).

⁷R. Shakeshaft and L. Spruch, *Rev. Mod. Phys.* **51**, 369 (1979).

⁸R. Abrines and I. C. Percival, *Proc. Phys. Soc. London* **88**, 873 (1966).

⁹R. E. Olson, K. H. Berkner, W. G. Graham, R. V. Pyle, A. S. Schlachter, and J. W. Stearns, *Phys. Rev. Lett.* **41**, 163 (1978).

¹⁰D. Banks, K. S. Barnes, and J. McB. Wilson, *J. Phys. B* **9**, L141 (1976).

¹¹P. J. Martin, D. M. Blankenship, T. J. Kvale, E. Redd, J. L. Peacher, and J. T. Park, *Phys. Rev. A* **23**, 3357 (1981).

¹²J. T. Park, J. E. Aldag, J. M. George, J. L. Peacher, and J. H. McGuire, *Phys. Rev. A* **15**, 508 (1977).

¹³I. C. Percival and D. Richards, *Adv. At. Mol. Phys.* **11**, 1 (1975).

¹⁴R. E. Olson and A. Salop, *Phys. Rev. A* **16**, 531 (1977).

¹⁵A. D. MacKellar and R. L. Becker (private communication).

- ¹⁶R. E. Olson, *Phys. Rev. A* **24**, 1726 (1981).
- ¹⁷C. F. Barnett, J. A. Ray, E. Ricci, M. I. Wilker, E. W. McDaniel, E. W. Thomas, and H. B. Gilbody, *Atomic Data for Controlled Fusion Research* (National Laboratory, Oak Ridge, Tennessee, 1977), p. A.4.2.
- ¹⁸D. Eichenauer, N. Grün, and W. Scheid, *J. Phys. B* **15**, L17 (1982).
- ¹⁹R. Shakeshaft, *Phys. Rev. A* **18**, 307 (1978).
- ²⁰M. B. Shah and H. B. Gilbody, *J. Phys. B* **14**, 2361 (1981).
- ²¹I. A. Sellin, *Electronic and Atomic Collisions*, edited by S. Datz (North-Holland, Amsterdam, 1982), pp. 195–221.
- ²²R. A. Phaneuf, F. W. Meyer, and R. H. McKnight, *Phys. Rev. A* **17**, 534 (1978).
- ²³H. J. Kim, R. A. Phaneuf, F. W. Meyer, and P. H. Stelson, *Phys. Rev. A* **17**, 854 (1978).
- ²⁴K. H. Berkner, W. G. Graham, R. V. Pyle, A. S. Schlachter, J. W. Stearns, and R. E. Olson, *J. Phys. B* **11**, 875 (1978).
- ²⁵K. H. Berkner, W. G. Graham, R. V. Pyle, A. S. Schlachter, and J. W. Stearns, *Phys. Rev. A* **23**, 2891 (1981).
- ²⁶M. B. Shah and H. B. Gilbody, *J. Phys. B* **15**, 413 (1982).
- ²⁷M. Rødbro and F. D. Andersen, *J. Phys. B* **12**, 2883 (1979).